BIOCHEMISTRY
including biophysical chemistry & molecular biology
Article

Biochemistry **2010,** *49,* 2705–2714 2705
DOI: 10.1021/bi100012u

Pyrophosphate Activation in Hypoxanthine−Guanine Phosphoribosyltransferase with Transition State Analogue†

Hua Deng,‡ Robert Callender,*,‡ Vern L. Schramm,‡ and Charles Grubmeyer§

‡*Department of Biochemistry, Albert Einstein College of Medicine, Bronx, New York 10461, and* §*Department of Biochemistry and Fels Institute for Cancer Research and Molecular Biology, Temple University School of Medicine, 3307 North Broad Street, Philadelphia, Pennsylvania 19140*

Received January 6, 2010; Revised Manuscript Received February 15, 2010

ABSTRACT: Isotope-edited difference Raman and FTIR studies complemented by *ab initio* calculations have been applied to the transition state analogue complex of HGPRT·ImmHP·$MgPP_i$ to determine the ionic states of the 5′-phosphate moiety of ImmHP and of PP_i. These measurements characterize electrostatic interactions within the enzyme active site as deduced from frequency shifts of the phosphate groups. The bound 5′-phosphate moiety of ImmHP is dianionic, and this phosphate group exists in two different conformations within the protein complex. In one conformation, a hydrogen bond between the 5′-phosphate of ImmHP and the OH group of Tyr104 in the catalytic loop appears to be stronger. With the stronger H-bond, the OH of Tyr104 approaches one of the P⋯O bonds from the bridging oxygen side to cause distortion of the PO_3 moiety, as indicated by a lowered symmetric P⋯O stretch frequency. The asymmetric stretch frequencies are similar in both phosphate conformations. Bound PP_i in this complex is fully ionized to $P_2O_7^{4-}$. Bond frequency changes for bound PP_i indicate coordination to Mg^{2+} ions but show no indication of significant P⋯O bond polarization. Extrapolation of these results to reaction coordinate motion for HGPRT suggests that bond formation between C1′ of the nucleotide ribose and the oxygen of PP_i is accomplished by migration of the ribocation toward immobilized pyrophosphate.

HGPRT[1] belongs to the type I phosphoribosyltransferase family of enzymes that catalyzes the displacement of pyrophosphate (PP_i) from α-D-5-phosphoribosyl 1-pyrophophate (PRPP) by nitrogen nucleophiles including ammonia, adenine, hypoxanthine, guanine, xanthine, orotate, or uracil to produce a β-substituted ribose 5′-phosphate and PP_i. Hypoxanthine−guanine phosphoribosyltransferases from humans and parasites catalyze the reversible Mg^{2+}-dependent transfer of the phosphoribosyl group from PRPP to hypoxanthine or guanine to form IMP or GMP nucleotides, respectively (see Scheme 1). The substrates bind in a functionally ordered fashion, with PRPP binding first in the forward direction and IMP or GMP first in the reverse reaction (*1*). This enzyme has been studied as a chemotherapeutic target for malaria, giardiases, trypanosomiasis, and toxoplasmosis (*2*, *3*). The feasibility to target *Trypanosoma cruzi* HGPRT, the agent of Chagas' disease, has been demonstrated (*4*). In humans, genetically impaired purine salvage by HGPRT is the basis for heritable gouty arthritis and, in severe cases, Lesch−Nyhan syndrome (*5*).

A detailed understanding of the structure and function of HGPRT is provided from analysis of nearly 30 crystal structures of human or parasite isozymes, including those complexed with a variety of ligands that resemble Michaelis, transition state, and product complexes (*1*, *6*−*17*). The crystal structures of HGPRT with a bound transition-state analogue show that a disordered catalytic loop moves up to 25 Å to cover the active site and becomes an ordered two-stranded, antiparallel β-sheet, as compared to its disordered state in the HGPRT·GMP·Mg^{2+} complex (*8*, *12*, *15*, *16*). A schematic drawing of active site contacts in the transition state analogue complex of human HGPRT is shown in Scheme 2.

Analysis of these crystal structures suggests a reaction coordinate with a relatively fixed purine ring and pyrophosphate but significantly different ribose ring conformations and positions on conversion of reactants to products. The pyrophosphate moiety is highly immobilized by its coordination with two Mg^{2+} ions and hydrogen bonds to active site Arg199, Lys68, and the backbone NH of Ser103. The position of the 5′-phosphate moiety is also fixed by numerous hydrogen bonds, including one from the conserved Tyr104 in the catalytic loop that closes the catalytic site upon substrate binding. The purine base is hydrogen bonded with conserved protein residues Asp137 and Lys165 and the carbonyl oxygen of Val187 (Scheme 2).

The transition state structure for phosphoribosyltransferases is based on results of kinetic isotope effect studies from the related orotate phosphoribosyltransferases from human, *Plasmodium falciparum*, and *Salmonella typhimurium* sources, using phosphonoacetate as a slowly reacting substrate analogue for pyrophosphate (Scheme 1 (*18*, *19*)). The transition state for *S. typhimurim* OPRTase is a dissociative structure with an elongated N1···C1′ bond (bond order of 0.3), minimal formation of the incoming C1′···O bond (bond order 0.02, from the pyrophosphate

†This work was supported in part by Grants EB001958 (H.D.), GM068036 (R.C.), GM41916 (V.L.S.), and GM52125 (C.G.) from the National Institutes of Health.

*To whom correspondence should be addressed: 718-430-3024 (phone); 718-430-8565 (fax); robert.callender@einstein.yu.edu (e-mail).

[1]Abbreviations: HGPRT, hypoxanthine−guanine phosphoribosyltransferase; OPRTase, orotate phosphoribosyltransferase; PNP, purine nucleoside phosphorylase; G6P, glucose 6-phosphate; PP_i, pyrophosphate; PRPP, α-D-5-phosphoribosyl 1-pyrophosphate; IMP, inosine 5′-monophosphate; GMP, guanosine 5′-monophosphate; ImmHP, immucillin-H 5′-phosphate; ImmGP, immucillin-G 5′-phosphate.

Published on Web 02/19/2010

Scheme 1: Reaction Catalyzed by HGPRT and Its Putative Transition State

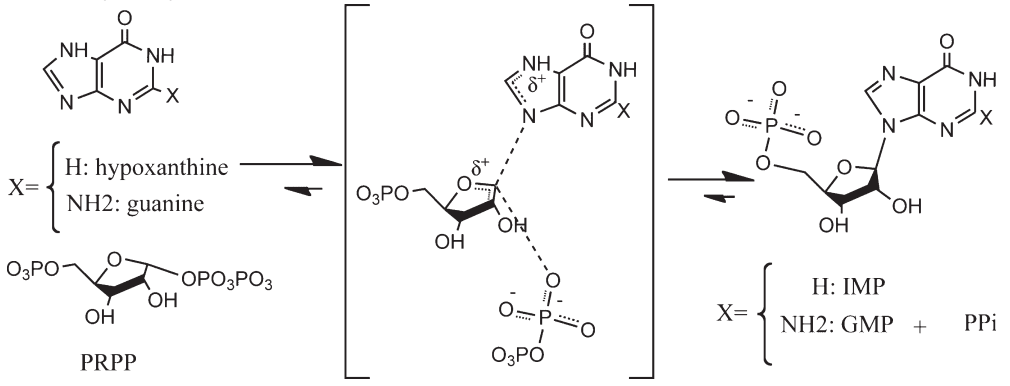

Scheme 2: Active Site Contacts in the HGPRT/ImmGP/PP_i Complex[a]

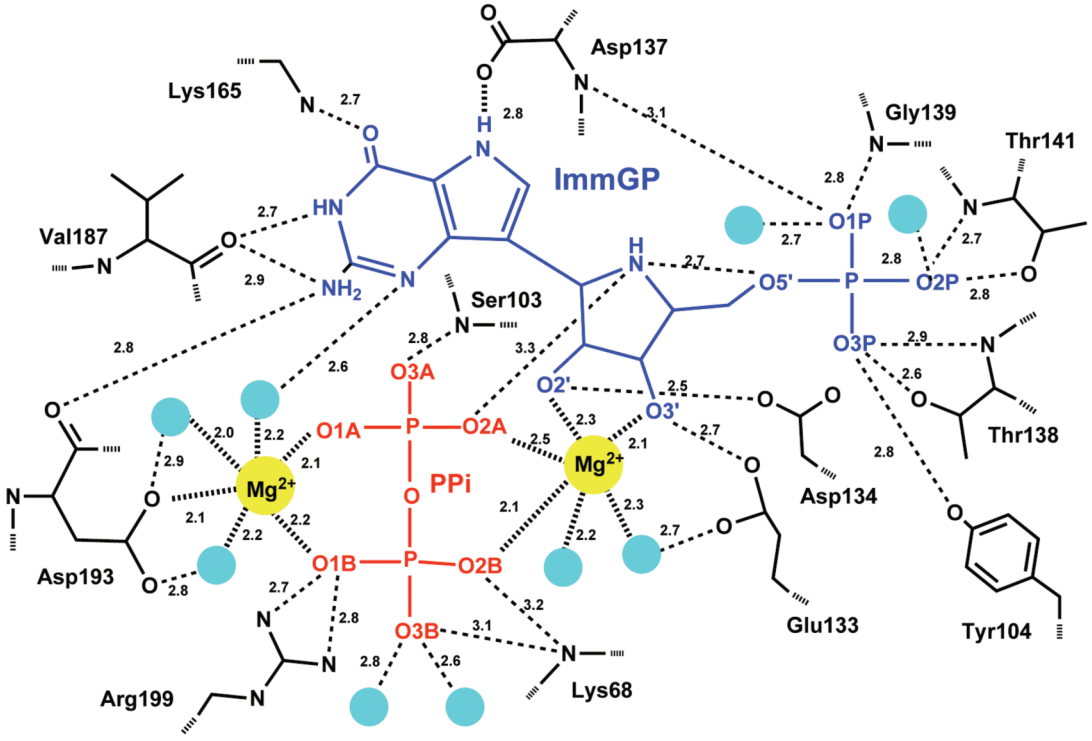

[a]Taken from ref *16*.

analogue), oxacarbenium ion character in the ribosyl group, and partial positive charge near C-1′. Human and *P. falciparum* OPRTases are also dissociative but with complete loss of the N1−C1′ bond and low bond order to the attacking nucleophile (*19*). Ionic stabilization for the transition state is proposed to come from the nearby pyrophosphate anion. In the case of HGPRTase, activation of the base may come from protein- or solvent-mediated protonation of N-7. From the crystal structures and the putative transition state structures, it has been suggested that the reaction catalyzed by HGPRT proceeds by a mechanism involving nucleophilic displacement by electrophile migration; both the purine and pyrophosphate nucleophiles are relatively fixed in position and the ribosyl group is converted to an oxacarbenium ion that migrates toward the purine base in the forward reaction or toward the pyrophosphate in the reverse direction (*20*).

Despite these extensive studies on HGPRT, some important mechanistic questions related to proton movements during catalysis remain to be answered. For example, high-resolution X-ray structural studies (at 1.05 Å) suggested a tight hydrogen bond between the OH group of Tyr104 in the catalytic loop and one of the 5′-phosphate oxygens of the substrate PRPP. The distance between the two oxygens is 2.67 Å in the HGPRT·9-deazaguanine·MgPRPP complex, and the hydrogen between the two oxygens was proposed to be part of a low-barrier H-bond (*12*). Thus, there is a possibility that the proton from the Tyr104 hydroxyl group may protonate the 5′-phosphate of the substrate at the transition state. The ionic states of PP_i in the HGPRT complexes are also unknown. Moreover, the crystal structures of HGPRT with transition state analogues show the bound PP_i with one of the three nonbridging P···O bonds on each phosphorus atom approximately 0.1 Å longer than the other two (PDB code 1BZY, 1CJB), suggesting a dianionic PP_i in the complex; however, the 2.0 Å resolution of these structures cannot be used with confidence to establish such small differences in PO bond lengths. These, and other important structural issues, can be addressed by vibrational spectroscopy. This approach is sensitive to the electronic nature of specific bonds. For example,

bond vibrational frequencies are strongly affected by protonation state. In addition, the characteristic time constant for vibrational spectroscopy is on the femtosecond scale. Hence, structural conformations interconverting on slower time scales are resolved in the vibrational spectrum as isolated bands. These frequencies are diagnostic of specific conformations, and band intensity is proportional to the concentration of each specific conformation.

In this study, isotope-edited FTIR and Raman difference techniques are used to determine the ionic states of the 5′-phosphate of immucillin-HP (ImmHP) and of PP_i in the HGPRT·ImmHP·$MgPP_i$ complex and to examine the extent of "activation" of the pyrophosphate nucleophile. ImmHP binds to human HGPRT 14000 times tighter than IMP, and this complex is considered to be a mimic of the HGPRT transition state (*16*). The evidence for this contention includes slow, tight binding behavior (*21*), the protonation states of N7 and N4′ (*22*), and striking immobilization of the peptide backbone (*23*).

MATERIALS AND METHODS

Monosodium and disodium glucose 6-phosphate and tetrasodium and disodium PP_i were purchased from Aldrich. ImmHP was prepared according published procedures (*24*). $^{18}O_3P$-labeled ImmHP was prepared using γ-$^{18}O_3$-labeled ATP as the phopsphoryl donor in ImmHP synthesis. ^{18}O-labeled PP_i was prepared according to the published procedure except the amount of [^{18}O]water added was reduced to maximize PP_i production (*25*). The product was purified through two cycles of AG1-X8, with elution by 150 mM HCl and neutralized with NaOH.

Enzyme Samples. Recombinant human HGPRT was expressed and purified to homogeneity as described previously (*26*). The purification method yielded an enzyme with undetectable alkaline phosphatase activity, permitting incubations with nucleotide ligands without phosphate loss. Purified HGPRT was stored at 4 °C in 0.1 M Tris-HCl (pH 7.4) containing ammonium sulfate at 70% saturation until ready to use for spectroscopic studies. The enzyme samples for spectroscopic measurements were prepared by extensive dialysis in 10 mM Tris at pH 7.5 with 10 mM $MgCl_2$ and 5 mM DTT, followed by concentration with a Centricon30 centrifuge (Amicon, Lexington, MA) to the desired concentration. In some cases, a second round of ion-exchange chromatography was performed to remove a slight fluorescent impurity. The concentrations of the HGPRT were determined spectroscopically, using a molar extinction coefficient of 26000 M^{-1} cm^{-1} at 280 nm. The HGPRT·ImmHP·$MgPP_i$ complex was prepared by adding a slight excess of ImmHP (or ^{18}O-labeled ImmHP) and PP_i (or ^{18}O-labeled PP_i) to the concentrated HGPRT sample. After 2 h the samples were washed twice with buffer in a Centricon30 concentrator. The binding of the ImmHP·$MgPP_i$ complex is tight (K_d = 1 nM (*21*)), and stoichiometric amounts of ImmHP·$MgPP_i$ bind to the HGPRT to form the transition state analogue complex. The typical concentration of enzyme−complex samples was 2 mM.

Difference Raman Spectroscopy. The Raman spectra were measured using an optical multichannel analyzer system consisting of a Triplemate spectrometer (Spex Industries, Metuchen, NJ) and a model DIDA-1000 reticon detector connected to an ST-100 detector (Princeton Instruments, Trenton, NJ) or a CCD detector (Princeton Instruments model LN/CCD-1152UV) connected to a ST-135 CCD controller. Details of the system can be found elsewhere (*27*). The 514.5 nm line from an argon ion laser or 568.2 nm line from a krypton ion laser was used to irradiate the sample (~100 mW).

Separate spectra for the HGPRT·ImmHP·$MgPP_i$ complex with and without ^{18}O labeling on ImmHP or PP_i were measured using a special split cell (the volume of each side being about 30 μL) and a sample holder with a linear translator as previously described (*27*). The spectrum from one side of the split cuvette was taken, the split cell was translated, and the spectrum from the other side was taken. This sequence was repeated until sufficient signal-to-noise ratio was achieved. A difference spectrum was generated by numerically subtracting the sum of the spectra obtained from each side. In general, the two summed spectra did not subtract to zero, as judged by the subtraction fidelity of know protein bands (for example, the amide I, amide III, and the sharp phenylalanine 1004 cm^{-1} bands, the latter band being especially useful since it is generally not affected by protein conformational changes). These protein bands were discerned from their band widths (generally much broader than those from spectra of bound substrates) and their characteristic positions. Hence, one summed spectrum was scaled by a small numerical factor, generally between 1.05 and 0.95, which was adjusted until the protein bands were nulled. The same control procedures were performed on all the difference spectra results herein. Resolution of the spectrometer is 8 cm^{-1} for the present results. Spectral calibration was done for each measurement using the known Raman lines of toluene, and absolute band positions are accurate to within ±2 cm^{-1}. None of the spectra presented here have been smoothed.

Difference FTIR Spectroscopy. FTIR spectroscopy was performed on a Magna 760 Fourier transform spectrometer (Nicolet Instrument Corp., WI) using a MCT (mercury−cadmium−telluride) detector. Enzyme ternary complexes with and without ^{18}O-labeled ImmHP or PP_i were simultaneously loaded into a two-position dual cell shuttle accessory. The FTIR spectra were taken alternatively between these two samples with BaF_2 windows and 15 μm Teflon spacers. Spectra were collected in the range of 900−4000 cm^{-1} with 2 cm^{-1} resolution. A Blackman−Harris three-term apodization and a Happ−Genzel apodization were applied, respectively. Omnic 4.1a (Nicolet Instrument Corp.) software was used for data collection and analysis. Since the sample and reference cells were assembled separately, their path lengths were not exactly equal. To correct for this, the subtracted spectrum was multiplied by a correction factor, typically in the range of 0.95−1.05.

Theoretical Calculations. *Ab initio* calculations were carried out on PP_i model compounds using the HF/6-31 g** functional, as implemented in Guassian 98. The geometries of the model compounds of tetra-, tri-, and dianionic PP_i were first optimized energetically, and the vibrational normal modes with Raman and IR intensities were calculated using the same basis set. True local minimum on the potential surface of the complexes for the geometry-optimized complexes were verified from the vibrational frequency calculations in which no imaginary frequency was found. In all cases, a stable structure of the model compound was achieved without any geometry constraints. The same calculations were also performed for the tetra- and dianionic PP_i complexed with two Na^+ ions to model the structure of PP_i in the HGPRT·ImmHP·$MgPP_i$ complex and to determine the effect of Mg^{2+} ions on the nonbridging P··O stretch frequencies.

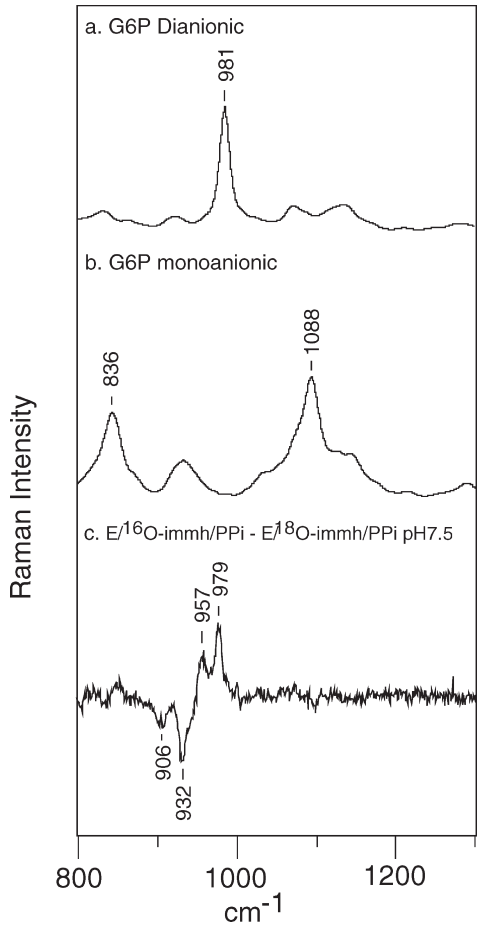

FIGURE 1: (a) Raman spectrum of 100 mM dianionic G6P at pH 8.5. (b) Raman spectrum of 100 mM monoanionic G6P at pH 4.0. (c) Raman difference spectrum between the HGPRT·ImmHP·$MgPP_i$ complex and HGPRT·^{18}O-ImmHP·$MgPP_i$ complex at a enzyme concentration of 2 mM. The enzyme samples were prepared in 10 mM Tris at pH 7.5 with 5 mM DTT. The 514.5 nm line from an argon ion laser or the 568.2 nm line from a krypton ion laser was used to irradiate the sample (~100 mW). The spectral resolution was 8 cm^{-1}.

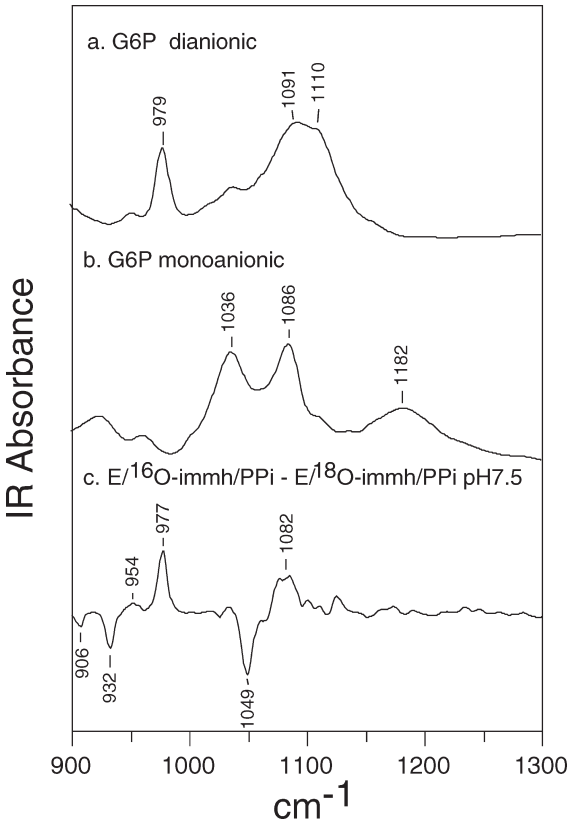

FIGURE 2: (a) FTIR spectrum of 100 mM G6P at pH 8.5. (b) FTIR spectrum of 100 mM G6P at pH 4.0. (c) FTIR difference spectrum between the HGPRT·ImmHP·$MgPP_i$ complex and HGPRT·^{18}O-ImmHP·$MgPP_i$ complex. The enzyme samples were the same as described in Figure 1. The spectral resolution was 2 cm^{-1}.

RESULTS AND DISCUSSION

Ionic State of the 5′-Phosphate Group of ImmHP in the Complex with HGPRT. The ionic state of the ImmHP 5′-phosphate group and its interaction with HGPRT were determined in difference Raman and FTIR measurements. The phosphate vibrational spectra of bound ligand are compared with solution model compounds. Since ImmHP is poorly soluble in common solvents, G6P was used in the phosphomonoester solution given the similarity of the phosphate groups in G6P and ImmHP. The Raman and FTIR spectra of G6P in aqueous solution at pH 8.5 characterize the dianionic phosphate moiety (spectra a in Figures 1 and 2). The band in the Raman spectrum at 981 cm^{-1} (Figure 1) is assigned to the symmetric stretch mode of the PO_3^{2-} moiety. This mode is also (weakly) IR active, appearing at 979 cm^{-1} (Figure 2). Vibrational studies of more than 20 phosphate monoester compounds in solution indicate that the frequency of this mode is 981 ± 5 cm^{-1} and is insensitive to the attached alcohol. An exception is glucose 1-phosphate, where it is 968 cm^{-1} (*28*). The bands at 1091 and 1110 cm^{-1} in the FTIR spectrum are assigned to the dianionic phosphate asymmetric stretch modes (Figure 2). In contrast to the symmetric stretch, the nearly degenerate asymmetric nonbridging P⋯O stretch modes are sensitive to the alcohol substituent, generally correlated with the pK_a of their OH groups. They also show unusually large heterogeneously broadened band widths (*28*). These modes are strongly IR active but only weakly Raman active. The average frequencies for the asymmetric modes range from 1098 cm^{-1} for glycerol-2-P to 1112 cm^{-1} for phosphoenolpyruvate (*28*).

The Raman and FTIR spectra of G6P at pH 4.0 (where the phosphate moiety of G6P is monoanionic) show the stretch motions of the two P−O single bonds to be coupled, forming a symmetric stretch and an asymmetric stretch (spectra b, Figures 1 and 2). The Raman active symmetric stretch mode is observed at 836 cm^{-1} (Figure 1b), and the IR active asymmetric mode is observed at 1036 cm^{-1} (Figure 2b). The two nonbridging P⋯O stretches couple to form a symmetric and an asymmetric stretch pair. The symmetric mode is both Raman and IR active and is observed at 1088 and 1086 cm^{-1} (Figures 1b and 2b, respectively). The asymmetric mode is only IR active and is assigned to the band at 1182 cm^{-1} (Figure 2b).

Since the vibrational spectra of mono- and dianionic phosphate are different, the ionic state of the phosphate monoester is readily identified by vibrational spectroscopy. The isotopically edited difference Raman and FTIR spectra for the HGPRT·ImmHP·$MgPP_i$ and HGPRT/^{18}O-ImmHP·$MgPP_i$ complexes reveal only the vibrational modes that are sensitive to labeling, with the protein contributions eliminated (spectrum c in Figures 1 and 2). Difference spectra are essential in these Raman studies since the band intensities from protein modes are comparable to or more intense than phosphate modes (*29*). The major Raman band at 979 cm^{-1} is assigned to the symmetric

nonbridging P⋯O stretch mode of the PO_3^{2-} group on ImmHP based on its shift upon ^{18}O labeling (Figure 1c). The assignment is also supported by the difference IR spectrum in which this band appears at 977 cm^{-1} (Figure 2c). The 1082 cm^{-1} band in Figure 2c is assigned to the asymmetric mode of the nonbridging P⋯O stretch mode of the PO_3^{2-} moiety of ImmHP in the ternary complex. This mode shifts down to 1049 cm^{-1} upon ^{18}O labeling.

Based on the vibrational spectroscopic measurements, the phosphate moiety of ImmHP in the HGPRT·ImmHP·$MgPP_i$ complex is dianionic. The symmetric nonbridging P⋯O stretch mode is near 980 cm^{-1}, characteristic of the dianionic phosphate. X-ray crystallographic structures are consistent with this interpretation since the lengths of all three nonbridging P⋯O bonds of ImmHP in ternary complexes are within 0.03 Å of each other (PDB code 1BZY, 1CJB).

Interactions between HGPRT and the 5′-Phosphate of ImmHP, a Transition State Analogue. The minor Raman band at 957 cm^{-1} (954 cm^{-1} in IR) can be assigned to the phosphate symmetric stretch mode since it is active in both Raman and IR and shifts down by about 50 cm^{-1} upon ^{18}O labeling (Figures 1c and 2c, respectively). As the stoichiometries of molecular species are proportional to signal strength in vibrational spectra, the simplest explanation for two 5′-phosphate symmetric stretch bands is two distinct conformations in the protein complex. Phosphate groups within the two conformations have similar asymmetric stretch frequencies but have different symmetric stretch frequencies. Previous studies of phosphate compounds based on molecular modeling with *ab initio* and empirical methods suggest that the symmetric stretch mode is sensitive to geometry (*30*). A small increase in the angle between adjacent P⋯O bonds would reduce the symmetric stretch frequency but leave the asymmetric stretch mode relatively unchanged (*30*). A structural explanation consistent with the data is for catalytic loops of the different protein subunits to have different hydrogen-bonding patterns with the 5′-phosphate. Different hydrogen bonds to the 5′-phosphate from Tyr104 OH would result in a variation of the 5′-phosphate O⋯P⋯O angles. Small distance differences, below the resolution of X-ray crystallography (*16*, *24*) can easily account for the observed spectral band pattern (*30*, *31*).

The frequency of the 5′-phosphate asymmetric stretch mode of ImmHP in the HGPRT·ImmHP·$MgPP_i$ complex is 1082 cm^{-1}, about 20 cm^{-1} lower than that of the solution model. Lowered stretch frequency correlates with reduced bond order of the nonbridging P⋯O bonds, indicating stronger hydrogen bonding to phosphate in the enzyme complex than in water. The enzyme environment also restricts the O⋯P⋯O angles compared to solution as shown by the narrow asymmetric P⋯O stretch bandwidth in the complex (Figure 2).

The Ionic State of PP_i in the Presence of a Transition State Analogue. Difference spectroscopic studies were also performed to determine the stretch mode frequencies of PP_i within the HGPRT·ImmHP·$MgPP_i$ complex, using ^{18}O-labeled and unlabeled PP_i. The results were compared to the solution spectra to establish phosphate ionic states within the enzyme complex. Many PP_i bands are broad in solution and are masked or appear shifted from their true position in difference spectra. Thus, Raman and FTIR spectra were analyzed for solution PP_i data. In the HGPRT·ImmHP·$MgPP_i$ complex, the PP_i bands are sharpened considerably. Here, difference Raman and FTIR spectra eliminate background protein bands and permit characterization of the enzyme complex.

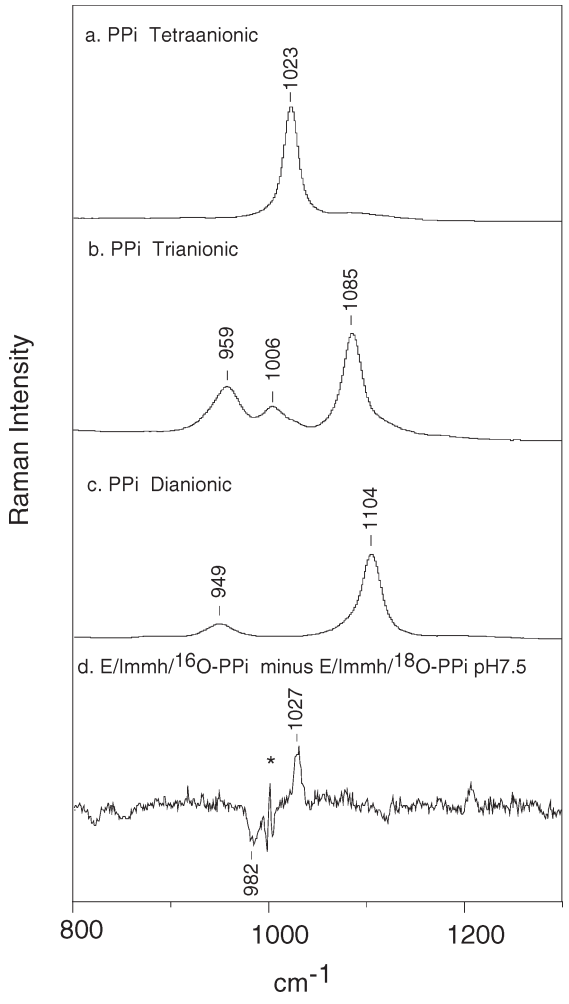

FIGURE 3: (a) Raman spectrum of 100 mM tetraanionic PP_i (pH 11). (b) Raman spectrum of trianionic PP_i. This spectrum is obtained by subtracting the appropriate amount of (a) and (c) from the spectrum of 100 mM PP_i at pH 7.5. (c) Raman spectrum of 100 mM dianionic PP_i (pH 4.5). (d) Raman difference spectrum between the HGPRT·ImmHP·$MgPP_i$ complex and HGPRT·ImmHP·Mg-^{18}O-PP_i complex. The experimental conditions were the same as described in Figure 1.

The Raman spectrum of tetraanionic PP_i, obtained from tetrasodium PP_i at pH 11, shows a major band at 1023 cm^{-1}, assigned to the in-phase combination of the two symmetric P⋯O stretch modes from both PO_3^{2-} moieties (spectrum a in Figure 3). This mode shifts down to 978 cm^{-1} upon ^{18}O labeling (data not shown) and is only active in the Raman spectrum. The bands at 1108 and 1136 cm^{-1} in the FTIR spectrum of tetraanionic PP_i are assigned to the asymmetric combinations of the P⋯O bond stretches (only IR active; spectrum a, Figure 4). The FTIR band at 915 cm^{-1} is assigned to the asymmetric P−O stretch mode of the bridging P−O−P bonds (IR active, Raman inactive; spectrum a, Figure 4). The assignments of the PP_i modes are supported by *ab initio* calculations on related model compounds (discussed below).

The Raman and FTIR spectra of dianionic PP_i, prepared from disodium PP_i at pH 4.5, are shown in spectrum c in Figures 3 and 4, respectively. The major Raman band at 1104 cm^{-1} is assigned to the in-phase combination of the two symmetric nonbridging P⋯O stretch modes from the two PO_2^- moieties (Figure 3c). This mode shifts down by 39 cm^{-1} to 1065 cm^{-1} upon ^{18}O labeling (data not shown) and is also observed in the IR spectrum

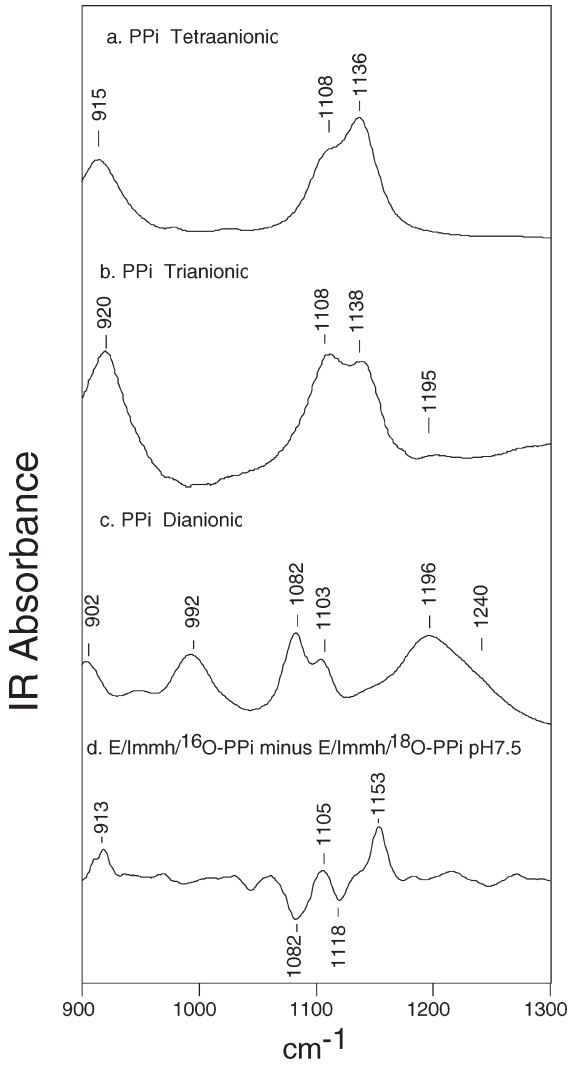

FIGURE 4: (a) FTIR spectrum of 100 mM tetraanionic PP_i (pH 11). (b) FTIR spectrum of 100 mM PP_i. This spectrum is obtained by subtracting the appropriate amount of (a) from the spectrum of 100 mM PP_i at pH 8.0. (c) FTIR spectrum of 100 mM dianionic PP_i (pH 4.5). (d) FTIR difference spectrum of the HGPRT·ImmHP·$MgPP_i$ complex and HGPRT·ImmHP·$Mg^{18}O$-PP_i complex. The experimental conditions were the same as described in Figure 2.

(Figure 4c). One of the major IR bands at 1196 cm^{-1} is assigned to the out-of-phase combination of the two symmetric nonbridging P⋯O stretches from the two PO_2^- moieties (Figure 4c). Another major IR band at 1082 cm^{-1} is assigned to an asymmetric stretch of the two terminal P−OH bond stretches. This mode is only IR active and shifts down by about 37 cm^{-1} to 1046 cm^{-1} upon ^{18}O labeling of PP_i (data not shown). The shoulder band at ∼1240 cm^{-1} is assigned to an asymmetric combination of the nonbridging P⋯O stretch mode. The band at 920 cm^{-1} is assigned to the asymmetric P−O stretch mode of the bridging P−O−P bonds, and this mode is only IR active (Figure 4c).

The Raman and FTIR spectra of trianionic PP_i are shown in spectrum b in Figures 3 and 4, respectively. For PP_i, pK_{a3} is 6.7, and pK_{a4} is 9.4, so that, at pH values between 7.5 and 8.0, PP_i is >80% trianionic. However, contributions from tetra- and dianionic PP_i in the original spectra were apparent and were subtracted to obtain the spectrum of trianionic PP_i presented here (spectrum b, Figures 3 and 4). In trianionic PP_i, there are five P⋯O bonds, and three of them are on one phosphorus and two on the other. The most prominent band in the Raman spectrum is at 1085 cm^{-1}. This band is assigned to the symmetric stretch mode of the two nonbridging P⋯O bonds on one phosphorus since this mode is expected to have the strongest Raman intensity. The Raman band at 1006 cm^{-1} in Figure 3b is tentatively assigned to the symmetric stretch of the three P⋯O bonds of the PO_3^{2-} moiety on the other phosphorus. These two modes, only Raman active, do not appear in the FTIR spectrum, supporting the assignment. The Raman band at 959 cm^{-1} (Figure 3b) is tentatively assigned to a combination of stretch motions of the single P−O bonds. The IR bands in Figure 4b at 1008, 1138, and 1195 cm^{-1} are assigned to various asymmetric combinations of nonbridging P⋯O stretch vibrations.

The difference Raman and FTIR spectra between HGPRT·ImmHP·$MgPP_i$ and HGPRT·ImmHP·$Mg^{18}O$-PP_i complexes are shown in spectra d of Figures 3 and 4, respectively. Only one Raman band is observed at 1027 cm^{-1} which shifts down by 45 cm^{-1} to 982 cm^{-1} upon ^{18}O labeling (spectrum d, Figure 3). The derivative feature marked with an asterisk in this spectrum is an artifact from imperfect subtraction of the sharp protein phenylalanine peak. Two asymmetric nonbridging P⋯O stretch modes are observed in the FTIR difference spectrum: one at 1153 cm^{-1}, which shifts down by 35 cm^{-1} to 1118 cm^{-1} upon ^{18}O labeling, and the other at 1105 cm^{-1} shifting down to 1082 cm^{-1} (spectrum d, Figure 4). The position of the second band cannot be accurately determined due to its partial cancellation from the 1118 cm^{-1} band of the ^{18}O-labeled PP_i. However, their bandwidths are much narrower than those of the model compounds in solution.

X-ray structures of HGPRT·ImmGP·$MgPP_i$ (where G represents 9-deazaguanine) and HGPRT·ImmHP·$MgPP_i$ are closely related and show two Mg^{2+} ions coordinated to bound PP_i. The X-ray structures suggest that one of the PO bonds of PP_i is about 0.1 Å longer than the other two PO bonds, but this difference is within the error limits for a structure at 2.0 Å resolution (PDF 1BZY (*16*)). This bond length difference is characteristic of dianionic PP_i. However, vibrational spectroscopic studies of PP_i in the HGPRT·ImmHP·$MgPP_i$ complex indicate that PP_i is in the tetraanionic state since the Raman active band at 1027 cm^{-1} (Figure 3d) is close to the band at 1023 cm^{-1} from solution tetraanionic PP_i (Figure 3a) but far from the major Raman band of other ionic forms. If PP_i were in a bound tri/dianionic form, PP_i would be expected to show a nonbridging P⋯O stretch mode that would have shifted down by 60−80 cm^{-1} in the Raman data (compare spectra b and c with spectrum d in Figure 3). To determine if such a shift is possible for P⋯O stretching modes, studies on the PP_i and Mg^{2+} ion interactions were performed by vibrational spectroscopic studies of PP_i/Mg^{2+} model compounds in solution and by *ab initio* calculations.

When PP_i is complexed with Mg^{2+}, nonbridging P⋯O stretch mode frequencies increase. With GDP as an example, the symmetric stretch mode of the αPO_2^- moiety at 1089 cm^{-1} (analogous to the 1085 cm^{-1} band in trianionic PP_i) is increased by 5 cm^{-1} in the MgGDP complex, and the two asymmetric stretch modes at 1115 and 1205 cm^{-1} (analogous to the 1138 and 1195 cm^{-1} bands in trianionic PP_i) are increased by 8 and 10 cm^{-1}, respectively, in the MgGDP complex (*32*). Spectra of PP_i complexed with Mg^{2+} in various ionic states show similar shifts of the nonbridging P⋯O stretch modes. For example, the

Scheme 3: Model PP_i Compounds Used in Vibrational Normal Mode Calculations

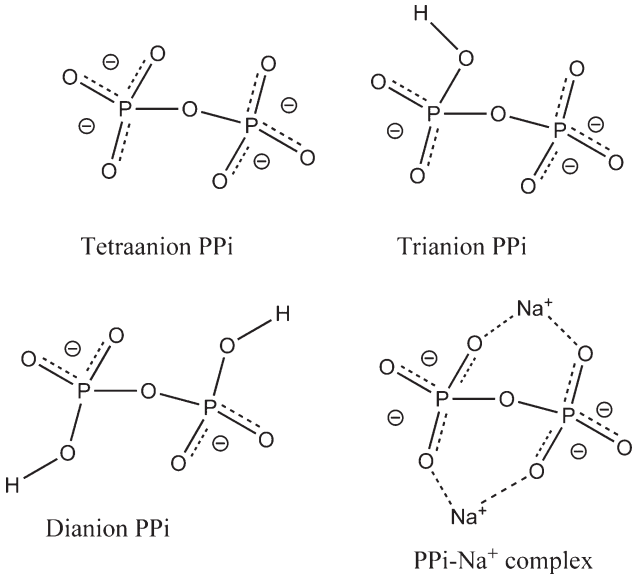

in-phase symmetric P··O stretch mode of tetraanionic PP_i at 1023 cm^{-1} (spectrum a, Figure 3) shifts up by 9 cm^{-1} in the $MgPP_i$ complex although the two asymmetric P··O stretch modes at 1108 and 1136 cm^{-1} (spectrum a, Figure 4) shift up by less than 2 cm^{-1} (data not shown). Thus, the interaction between Mg^{2+} and PP_i in solution causes a small upward shift (up to 15 cm^{-1}) in the nonbridging P··O stretch modes. However, it is also clear that interactions similar to those in solution cannot cause the 60−80 cm^{-1} downward shift of the symmetric stretch mode of the tri/dianionic PP_i if we assume the PP_i bound in HGPRT·ImmHP·$MgPP_i$ is tri/dianionic.

Theoretical Calculations. Vibrational analyses using *ab initio* methods on model compounds for PP_i and their Mg^{2+} complexes were used to determine if the Mg^{2+}−PP_i interactions suggested by X-ray crystallographic studies can induce the observed nonbridging P··O stretch mode frequency changes from solution to the HGPRT complex. The tetra-, tri-, and dianionic forms of PP_i were used to model their respective solution compounds, and the results of the calculations were then evaluated against the experimentally observed values. The tetra- and dianionic PP_i complexed with two sodium ions are used to model Mg^{2+}−PP_i interaction in HGPRT·ImmHP·$MgPP_i$ for reasons discussed below.

Since there is a high degree of symmetry in all ionic states of PP_i, group theory can be applied to predict Raman and IR intensities of the PO stretch modes. Group theory predicts that the most prominent bands in the Raman spectrum should be the in-phase combination of the two symmetric nonbridging P··O stretch modes of the PO_3^{2-} groups for tetraanionic PP_i and of the PO_2^- groups for dianionic PP_i because the motions of these modes maintain the symmetry of the molecule. These modes are easily identified in the Raman spectra and from calculations. They are also sensitive to the ionic state of PP_i, and thus we focus our attention on these modes (see Scheme 3).

The PP_i models were first optimized at the HF/6-31 g** level, and the vibrational frequencies with their Raman and IR intensities were calculated with the same basis set. These calculations overestimate the stretching force constants by about 20% and frequencies by about 10% (*33*, *34*). The coupling constants among nonbridging P··O stretches are also overestimated,

Table 1: Experimentally Observed Nonbridging P··O Stretch Modes in Tetra-, Tri-, and Dianionic and HGPRT-Bound PP_i[a]

	normal modes			
	ν_s	ν_{a1}	ν_{a2}	ν_{a3}
$P_2O_7^{4-}$	1023	1108	1136	
$P_2O_7H^{3-}$	1006, 1085	1108	1138	1195
$P_2O_7H_2^{2-}$	1104	1196		1240
in the complex	1027	1105	1153	

[a] ν_s is the Raman active symmetric nonbridging P··O stretches observed in the Raman spectra. ν_as are the IR active asymmetric combination of the nonbridging P··O stretches. All frequencies are in cm^{-1}.

Table 2: Calculated Nonbridging P··O Stretch Modes in Tetra-, Tri-, and Dianionic PP_i as Well as the Tetra- and Dianionic PP_i Complexed with Two Na^+[a]

	normal modes			
model	ν_s	ν_{a1}	ν_{a2}	ν_{a3}
$P_2O_7^{4-}$	1039	1163	1172	1178
+2Na^+	1042	1070	1279	1294
$P_2O_7H^{3-}$	1052, 1161	1209	1259	1293
$P_2O_7H_2^{2-}$	1179	1180	1343	1360
+2Na^+ (1)	1213	1177	1360	1438
+2Na^+ (2)	1230	1175	1320	1354
+2Na^+ (3)	1207	1130	1442	1461

[a] ν_s is the in-phase combination of the two symmetric P··O stretches from the two PO_3^{2-} and two PO_2^- groups in tetra- and dianionic PP_i, respectively. For trianionic PP_i, one symmetric P··O stretch from PO_3^{2-} and one from PO_2^- are listed as ν_s. ν_as are the asymmetric P··O stretch modes with the highest IR intensities as calculated by *ab initio* methods. All frequencies are in cm^{-1}. The two Na^+s in the model were positioned approximately at equal distances from the two phosphorus atoms. In model 1 of the dianionic $NaPP_i$ complex, one P−OH bond pointed away from the two Na^+ ions, and the other P−OH bond pointed approximately toward the Na^+ ions. In model 2, both P−OH bonds pointed away from Na^+ ions. In model 3, both P−OH bonds pointed approximately toward Na^+ ions.

resulting in a larger frequency separation between symmetric and asymmetric stretch modes than is measured. Another source of computational of error arises from the neglect of solvent. The interaction of water with PP_i decreases nonbridging P··O stretch frequencies. However, the errors are mostly uniform, and we are more interested in the frequency change when Mg^{2+} ions are complexed with PP_i. The errors in the absolute frequencies yielded by the calculations do not affect our conclusions. Similar frequency calculations on the phosphate compounds at MP2/6-31 g** or B3LYP/6-31 g** levels yielded better agreement with the experimental values for asymmetric stretch but worse on the symmetric stretch frequencies, and on average, no significant improvements over HF calculations were observed (*22*). Thus, they were not explored further.

The experimentally observed nonbridging P··O stretch frequencies in Raman and FTIR spectra of PP_i in various ionic states and in the HGPRT·ImmHP·$MgPP_i$ complex are compared (Table 1, Figures 3 and 4). The calculated frequencies of the nonbridging P··O stretch modes of various PP_i model compounds are shown in Table 2. For tetraanionic PP_i, there are six nonbridging P··O stretch modes from the six P··O bonds. The calculations suggest that two of the modes do not have significant intensity in either Raman or IR spectra. The calculated Raman active mode is the in-phase combination of the two symmetric P··O stretches of the two PO_3^{2-} groups with a

frequency of 1039 cm^{-1}. The calculations also predict that three of the five asymmetric combinations of the P⋯O stretches at 1163, 1172, and 1178 cm^{-1} have significant IR intensity (Table 2). The calculated frequency of the in-phase P⋯O stretch mode is less that 20 cm^{-1} higher than the experimentally observed value, but the calculated frequencies of the asymmetric modes are 40−50 cm^{-1} higher.

In trianionic PP_i, there are five nonbridging P⋯O stretch modes. The calculations suggest two Raman active modes from the two symmetric P⋯O stretch modes at 1052 and 1161 cm^{-1} of the PO_3^{2-} and PO_2^- moiety, respectively. The calculations also predict that all three asymmetric combinations of the P⋯O stretches at 1209, 1259, and 1293 cm^{-1} have significant IR intensity (listed in Table 2). The calculated frequency of the symmetric P⋯O stretch mode from PO_3^{2-} is ∼40 cm^{-1} higher than the experimentally observed frequency (1006 cm^{-1}), but all other calculated frequencies are ∼100 cm^{-1} higher. Since the errors are quite uniform among different vibrational modes, we can make the assignments of the observed Raman and IR bands based on these calculations.

In dianionic PP_i, there are four nonbridging P⋯O stretch modes. The calculated Raman active mode is the in-phase combination of the two symmetric P⋯O stretches of two PO_2^- moieties, and its frequency is at 1179 cm^{-1}. The calculated frequencies for asymmetric P⋯O stretch modes are at 1180, 1343, and 1360 cm^{-1}, respectively (Table 2). The calculated frequency of the in-phase P⋯O stretch mode is about 70 cm^{-1} higher than the experimentally observed value, and the calculated frequencies of the asymmetric modes are 20−100 cm^{-1} higher.

Although the calculations overestimate the nonbridging P⋯O stretch frequencies of PP_i, the order of the frequencies is maintained not only within the same ionic state but also among different ionic states. Thus, additional calculations on tetra- and dianionic PP_i complexed with two Na^+ ions are expected to provide reliable information about the effect of Mg^{2+}−PP_i interactions on the nonbridging P⋯O stretch modes. Na^+ ions rather than Mg^{2+} ions were used because both of the two Mg^{2+} ions in the HGPRT complex are also coordinated with four other ligands (see Scheme 2), and its electronic effects on PP_i are reduced as a consequence.

Two Na^+ ions were placed near the bridging oxygens between the two phosphorus atoms of PP_i, similar to the positions of Mg^{2+} found in the X-ray structures. The geometry of the complex was then optimized, and the frequencies were calculated from the optimized geometry. In the optimized geometry for dianionic PP_i complexed with Na^+, the P−O(H) bond lengths are about 0.1 Å longer than the nonbridging P⋯O bonds, the same as the difference in the bond lengths of the PO bonds in the X-ray structure of the HGPRT·ImmGP·$MgPP_i$ complex (2.0 Å resolution, 1BZY (*16*)). In the tetraanionic PP_i−Na^+ complex, the length differences among the nonbridging P⋯O bonds were less than 0.04 Å, similar to that of the 5′-phosphate group of ImmGP in the X-ray structure of the HGPRT·ImmGP·$MgPP_i$ complex. Calculations on the tetraanionic PP_i−Na^+ complex indicate that the Raman active in-phase symmetric P⋯O stretch mode would shift up by only 3 cm^{-1} while the IR active asymmetric stretch modes shift by about 100 cm^{-1} in both up and down directions (Table 2). Three different models were used for dianionic PP_i−Na^+ complexes: The geometry of the first was constructed with one P−OH bond pointing away from both Na^+ ions and another P−OH bond pointing approximately toward one Na^+. A second model had both P−OH bonds pointed away from Na^+ ions. The third had each P−OH pointing approximately toward a Na^+ ion. In each of the three models, the in-phase symmetric P⋯O stretch mode was shifted up by 30 cm^{-1} or more compared to isolated dianionic PP_i. The asymmetric modes were shifted either up or down depending on the model (Table 2).

Changes of the PP_i P⋯O stretch modes upon binding to HGPRT·ImmHP·$MgPP_i$ are best simulated by the tetraanionic $NaPP_i$ model. The frequency of the in-phase symmetric stretch mode shifts up by a few cm^{-1}, and the highest frequency asymmetric stretch mode shifts up by more. Dianonic PP_i in the HGPRT·ImmHP·$MgPP_i$ complex can be eliminated as the in-phase P⋯O stretch mode would be expected to shift down by about 70 cm^{-1} compared to that in solution (Table 1). This shift is not possible in the complex with two Mg^{2+} ions since experiments and calculations indicated that the effect of the Mg^{2+} on dianionic PP_i would be to shift the in-phase P⋯O stretch mode to higher frequency. Thus, we conclude that tetraionic PP_i is bound in the HGPRT·ImmHP·$MgPP_i$ complex.

CONCLUSION

Isotope-edited difference Raman and FTIR spectroscopies permit the assignment of the ionic states of the phosphate groups in the HGPRT·ImmHP·$MgPP_i$ complex. The 5′-phosphate group of ImmHP is dianionic and exists in two different conformations. One explanation is that the hydrogen bond between the 5′-phosphate of ImmHP and the OH of Tyr104 in the catalytic loop is slightly stronger in half of the subunits. As the Tyr-OH approaches one of the P⋯O bonds from the bridging oxygen side, it likely causes some flattening of the PO_3 moiety, as indicated by a lowered symmetric P⋯O stretch frequency and a lowered average P⋯O frequency. Bound PP_i is tetraanionic. The frequency changes for enzyme-bound PP_i are consistent with coordination to Mg^{2+} ions but show no indication of significantly polarized P⋯O bonds. In this structural mimic of the transition state for HGPRT, PP_i bond polarization by interaction with the cationic iminoribitol group of ImmHP is negligible.

Vibrational studies of purine nucleoside phosphorylase (PNP), a related enzyme, with the nonphosphorylated transition state analogue ImmH and phosphate have shown that the phosphate resembles a highly activated nucleophile with distorted P−O bond geometry similar to the transition state. One of the nonbridging P⋯O bonds is sufficiently polarized by enzyme active site interactions to cause its stretch motions to become decoupled from the motions of the other two P⋯O bonds (*22*). X-ray structures of the PNP complex suggest that the strong P⋯O bond polarization of the phosphate nucleophile is induced by combined electrostatic and hydrogen-bonding interactions from the 3′-OH of the analogue and the positively charged iminoribitol cation of ImmH (*35*, *36*). In the X-ray structures of the HGPRT·ImmHP·$MgPP_i$ complex, one of the pyrophosphate P⋯O bonds also forms hydrogen-bonding and electrostatic interactions with the 3′-OH and with the iminoribitol cation of ImmHP. The oxygen of this P⋯O bond also coordinates with one of the active site Mg^{2+} ions (see Scheme 2). Thus, a strong polarization of this P⋯O bond might be expected. However, the vibrational spectra do not support a polarized P⋯O bond in the HGPRT·ImmHP·$MgPP_i$ complex. All P⋯O stretch frequencies from PP_i shift to somewhat higher values compared with the solution frequencies, consistent with coordination to Mg^{2+} ions without additional polarization (see above). The X-ray structures of HGPRT·ImmHP·$MgPP_i$ revealed two factors to explain the

lack of polarization. The Mg^{2+} ion coordinated with the P··O bond is almost perpendicular to the P··O bond orientation, and the iminoribitol cation is 3.3 Å from the O2A oxygen of PP_i (see Scheme 2). This distance is 0.3 Å longer than the similar ionic interaction between the iminoribitol cation of ImmH and the activated oxygen of phosphate bound in the PNP·ImmH·phosphate complex (*37*). These features indicate that the HGPRT·ImmHP·$MgPP_i$ complex in HGPRT differs from the PNP·ImmH·phosphate complex. The nonpolarized P··O bond of the HGPRT complex suggests more leaving group activation or weaker similarity to the transition state in the HGPRT complex than that in the PNP complex phosphate and ImmH. This hypothesis is supported by a K_m/K_i ratio of 690000 for PNP but only 14000 for human HGPRT in complexes with ImmH (*26*, *38*).

ACKNOWLEDGMENT

We are grateful to Dr. Beth L. Pietrak for making the enzyme used in this study.

REFERENCES

1. Xu, Y., Eads, J., Sacchettini, J. C., and Grubmeyer, C. (1997) Kinetic mechanism of human hypoxanthine-guanine phosphoribosyltransferase: rapid phosphoribosyl transfer chemistry. *Biochemistry 36*, 3700–3712.
2. Ullman, B., and Carter, D. (1995) Hypoxanthine-guanine phosphoribosyltransferase as a therapeutic target in protozoal infections. *Infect. Agents Dis. 4*, 29–40.
3. Wang, C. C. (1984) Parasite enzymes as potential targets for antiparasitic chemotherapy. *J. Med. Chem. 27*, 1–9.
4. Freymann, D. M., Wenck, M. A., Engel, J. C., Feng, J., Focia, P. J., Eakin, A. E., and Craig, S. P. (2000) Efficient identification of inhibitors targeting the closed active site conformation of the HPRT from *Trypanosoma cruzi*. *Chem. Biol. 7*, 957–968.
5. Sculley, D. G., Dawson, P. A., Emmerson, B. T., and Gordon, R. B. (1992) A review of the molecular basis of hypoxanthine-guanine phosphoribosyltransferase (HPRT) deficiency. *Hum. Genet. 90*, 195–207.
6. Balendiran, G. K., Molina, J. A., Xu, Y., Torres-Martinez, J., Stevens, R., Focia, P. J., Eakin, A. E., Sacchettini, J. C., and Craig, S. P., III (1999) Ternary complex structure of human HGPRTase, PRPP, Mg^{2+}, and the inhibitor HPP reveals the involvement of the flexible loop in substrate binding. *Protein Sci. 8*, 1023–1031.
7. Guddat, L. W., Vos, S., Martin, J. L., Keough, D. T., and de Jersey, J. (2002) Crystal structures of free, IMP-, and GMP-bound *Escherichia coli* hypoxanthine phosphoribosyltransferase. *Protein Sci. 11*, 1626–1638.
8. Canyuk, B., Focia, P. J., and Eakin, A. E. (2001) The role for an invariant aspartic acid in hypoxanthine phosphoribosyltransferases is examined using saturation mutagenesis, functional analysis, and X-ray crystallography. *Biochemistry 40*, 2754–2765.
9. Kanaani, J., Somoza, J. R., Maltby, D., and Wang, C. C. (1996) Probing the active site of *Tritrichomonas foetus* hypoxanthine-guanine-xanthine phosphoribosyltransferase using covalent modification of cysteine residues. *Eur. J. Biochem. 239*, 764–772.
10. Somoza, J. R., Chin, M. S., Focia, P. J., Wang, C. C., and Fletterick, R. J. (1996) Crystal structure of the hypoxanthine-guanine-xanthine phosphoribosyltransferase from the protozoan parasite *Tritrichomonas foetus*. *Biochemistry 35*, 7032–7040.
11. Munagala, N., Basus, V. J., and Wang, C. C. (2001) Role of the flexible loop of hypoxanthine-guanine-xanthine phosphoribosyltransferase from *Tritrichomonas foetus* in enzyme catalysis. *Biochemistry 40*, 4303–4311.
12. Heroux, A., White, E. L., Ross, L. J., Kuzin, A. P., and Borhani, D. W. (2000) Substrate deformation in a hypoxanthine-guanine phosphoribosyltransferase ternary complex: the structural basis for catalysis. *Structure 8*, 1309–1318.
13. Heroux, A., White, E. L., Ross, L. J., Davis, R. L., and Borhani, D. W. (1999) Crystal structure of *Toxoplasma gondii* hypoxanthine-guanine phosphoribosyltransferase with XMP, pyrophosphate, and two Mg(2+) ions bound: insights into the catalytic mechanism. *Biochemistry 38*, 14495–14506.
14. Heroux, A., White, E. L., Ross, L. J., and Borhani, D. W. (1999) Crystal structures of the *Toxoplasma gondii* hypoxanthine-guanine phosphoribosyltransferase-GMP and -IMP complexes: comparison of purine binding interactions with the XMP complex. *Biochemistry 38*, 14485–14494.
15. Focia, P. J., Craig, S. P., III, Nieves-Alicea, R., Fletterick, R. J., and Eakin, A. E. (1998) A 1.4 Å crystal structure for the hypoxanthine phosphoribosyltransferase of *Trypanosoma cruzi*. *Biochemistry 37*, 15066–15075.
16. Shi, W., Li, C. M., Tyler, P. C., Furneaux, R. H., Grubmeyer, C., Schramm, V. L., and Almo, S. C. (1999) The 2.0 Å structure of human hypoxanthine-guanine phosphoribosyltransferase in complex with a transition-state analog inhibitor. *Nat. Struct. Biol. 6*, 588–593.
17. Eads, J. C., Scapin, G., Xu, Y., Grubmeyer, C., and Sacchettini, J. C. (1994) The crystal structure of human hypoxanthine-guanine phosphoribosyltransferase with bound GMP. *Cell 78*, 325–334.
18. Tao, W., Grubmeyer, C., and Blanchard, J. S. (1996) Transition state structure of *Salmonella typhimurium* orotate phosphoribosyltransferase. *Biochemistry 35*, 14–21.
19. Zhang, Y., Luo, M., and Schramm, V. L. (2009) Transition state of *Plasmodium falciparem* and human orotate phosphoribosyltransferases. *J. Am. Chem. Soc. 131*, 4685–4694.
20. Schramm, V. L., and Grubmeyer, C. (2004) Phosphoribosyltransferase mechanisms and roles in nucleic acid metabolism. *Prog. Nucleic Acid Res. Mol. Biol. 78*, 261–304.
21. Li, C. M., Tyler, P. C., Furneaux, R. H., Kicska, G., Xu, Y., Grubmeyer, C., Girvin, M. E., and Schramm, V. L. (1999) Transition-state analogs as inhibitors of human and malarial hypoxanthine-guanine phosphoribosyltransferases. *Nat. Struct. Biol. 6*, 582–587.
22. Deng, H., Lewandowicz, A., Schramm, V. L., and Callender, R. (2004) Activating the phosphate nucleophile at the catalytic site of purine nucleoside phosphorylase: a vibrational spectroscopic study. *J. Am. Chem. Soc. 126*, 9516–9517.
23. Wang, F., Shi, W., Nieves, E., Angeletti, R. H., Schramm, V. L., and Grubmeyer, C. (2001) A transition state analogue reduces protein dynamics in hypoxanthine-guanine phosphoribosyltransferase. *Biochemistry 40*, 8043–8054.
24. Shi, W., Li, C. M., Tyler, P. C., Furneaux, R. H., Cahill, S. M., Girvin, M. E., Grubmeyer, C., Schramm, V. L., and Almo, S. C. (1999) The 2.0 Å structure of malarial purine phosphoribosyltransferase in complex with a transition-state analogue inhibitor. *Biochemistry 38*, 9872–9880.
25. Hackney, D. D., Stempel, K. E., Boyer, P. D., and Daniel, L. P. (1980) Oxygen-18 probes of enzymic reactions of phosphate compounds, in Methods in Enzymology, pp 60−83, Academic Press, New York.
26. Xu, Y., and Grubmeyer, C. (1998) Catalysis in human hypoxanthine-guanine phosphoribosyltransferase: Asp 137 acts as a general acid/base. *Biochemistry 37*, 4114–4124.
27. Callender, R., and Deng, H. (1994) Nonresonance Raman difference spectroscopy: a general probe of protein structure, ligand binding, enzymatic catalysis, and the structures of other biomacromolecules. *Annu. Rev. Biophys. Biomol. Struct. 23*, 215–245.
28. Cheng, H., Nikolic-Hughes, I., Wang, J. H., Deng, H., O'Brien, P. J., Wu, L., Zhang, Z. Y., Herschlag, D., and Callender, R. (2002) Environmental effects on phosphoryl group bonding probed by vibrational spectroscopy: implications for understanding phosphoryl transfer and enzymatic catalysis. *J. Am. Chem. Soc. 124*, 11295–11306.
29. Deng, H., Ray, W. J., Jr., Burgner, J. W., Jr., and Callender, R. (1993) Comparison of vibrational frequencies of critical bonds in ground-state complexes and in a vanadate-based transition-state analog complex of muscle phosphoglucomutase. Mechanistic implications. *Biochemistry 32*, 12984–12992.
30. Deng, H., Wang, J., Ray, W. J., and Callender, R. (1998) Relationship between bond stretching frequencies and internal bonding for $[^{16}O_4]$ and $[^{18}O_4]$ phosphates in aqueous solution. *J. Phys. Chem. B 102*, 3617–3623.
31. Ray, W. J., Jr., Burgner, J. W., Jr., Deng, H., and Callender, R. (1993) Internal chemical bonding in solutions of simple phosphates and vanadates. *Biochemistry 32*, 12977–12983.
32. Wang, J. H., Xiao, D. G., Deng, H., Callender, R., and Webb, M. R. (1998) Vibrational study of phosphate modes in GDP and GTP and their interaction with magnesium in aqueous solution. *Biospectroscopy 4*, 219–227.
33. Hehre, W. J., Radom, L., Schleyer, P. v. R., and Pople, J. A. (1986) ab-initio Molecular Orbital Theory, Wiley, New York.
34. Pulay, P., Fogarasi, G., Pongor, G., Boggs, J. E., and Vargha, A. (1983) Combination of theoretical ab initio and experimental

information to obtain reliable harmonic force constants. Scaled quantum mechanical (SQM) force fields for glyoxal, acrolain, butadiene, formaldehyde, and ethylene. *J. Am. Chem. Soc. 105*, 7037–7047.
35. Shi, W., Basso, L. A., Santos, D. S., Tyler, P. C., Furneaux, R. H., Blanchard, J. S., Almo, S. C., and Schramm, V. L. (2001) Structures of purine nucleoside phosphorylase from *Mycobacterium tuberculosis* in complexes with immucillin-H and its pieces. *Biochemistry 40*, 8204–8215.
36. Fedorov, A., Shi, W., Kicska, G., Fedorov, E., Tyler, P. C., Furneaux, R. H., Hanson, J. C., Gainsford, G. J., Larese, J. Z., Schramm, V. L., and Almo, S. C. (2001) Transition state structure of purine nucleoside phosphorylase and principles of atomic motion in enzymatic catalysis. *Biochemistry 40*, 853–860.
37. Lewandowicz, A., Shi, W., Evans, G. B., Tyler, P. C., Furneaux, R. H., Basso, L. A., Santos, D. S., Almo, S. C., and Schramm, V. L. (2003) Over-the-barrier transition state analogues and crystal structure with *Mycobacterium tuberculosis* purine nucleoside phosphorylase. *Biochemistry 42*, 6057–6066.
38. Murkin, A. S., Birck, M. R., Rinaldo-Matthis, A., Shi, W., Taylor, E. A., Almo, S. C., and Schramm, V. L. (2007) Neighboring group participation in the transition state of human purine nucleoside phosphorylase. *Biochemistry 46*, 5039–5049.